BNL-94881-2011-JA

KINETICS OF HETEROGENEOUS NUCLEATION IN SUPERSATURATED VAPOR: FUNDAMENTAL LIMITS TO NEUTRAL PARTICLE DETECTION REVISITED

McGraw, R., Wang, J., and Kuang, C.

Submitted to Aerosol Sci. Technol.

March 2011

Atmospheric Sciences Division/Environmental Sciences Dept.

Brookhaven National Laboratory

U.S. Department of Energy
Office of Science

DISCLAIMER

Kinetics of heterogeneous nucleation in supersaturated vapor: Fundamental limits to neutral particle detection revisited

Robert McGraw, Jian Wang, and Chongai Kuang

Environmental Sciences Department, Atmospheric Sciences Division, Brookhaven National Laboratory, 11973, New York, USA

Abstract

We examine the nucleated (with barrier) activation of perfectly wetting (zero contact angle) particles ranging from essentially bulk size down to approximately one nanometer mass diameter. While similar studies trace back to the pioneering work of Fletcher [1958], we present here a novel approach to the analysis based on general area constructions that enable key thermodynamic properties including surface and bulk contributions to nucleation work to be interpreted geometrically with reference to the Kelvin curve. The kinetics of activation is described in more detail in terms of the mean first passage time (MFPT) for barrier crossing. MFPT theory and benchmark calculations are used to develop and test a new approximate but simpler to use analytic expression for barrier crossing rate. The present study is motivated by recent condensation particle counter (CPC) studies that appear to finally establish the long-predicted detection of "sub-Kelvin" particles in the nano-size regime. Corresponding states thermodynamic and kinetic scaling approaches are used to facilitate the correlation and selection of optimal CPC working fluids and operating conditions based on a new metric for heterogeneous nucleation, the signal to noise ratio, and on physical and chemical properties.

Keywords: nucleation kinetics, heterogeneous nucleation, barrier crossing, neutral particle detection, mean first passage time

1. Introduction

Striking advance has been made over the past several years in condensation particle counter (CPC) development, enabling particles in the sub-3 nm diameter range approaching the size of molecular clusters to be routinely detected in the laboratory [Winkler et al. 2008; Iida et al., 2009; Sipila et al., 2009; Vanhanen et al. 2010] and in the atmosphere [Jiang et al., 2010]. This instrumental breakthrough calls for a re-examination of the foundations of heterogeneous nucleation theory, still largely based on the capillarity approximation [Fletcher, 1958], wherein even small clusters are modeled as bulk-property liquid drops, and simplified kinetics. Fletcher's theory predicts heterogeneous nucleation, driven by thermal fluctuations, for the activation of very small particles (less than about 6 nm) whereas larger particles undergo a barrierless growth transition at the Kelvin limit. Activation by nucleation below the Kelvin limit is a key factor in lowering detection size, but only recently has the process been definitively observed [Winkler et al., 2008]. Another important development has been the screening of multiple CPC working fluids for optimal detector performance in the sub-3 nm regime [Magnusson et al., 2003; Iida et al., 2009].

The present study has several objectives beginning with re-examination of the theory. Any improvement over Fletcher's analysis is not easily done. One can contemplate a first-principles molecular simulation, but for an accurate prediction of nucleation rate this requires more realistic model potentials than are presently available. Molecular dynamics- and Monte Carlo-based simulations of nucleation are most useful where precision is enough – e.g. for identifying even small systematic departures from classical nucleation theory – but such simulations are beyond the scope of the present

study. Instead, we continue to rely on the capillarity approximation for estimating the thermodynamic properties needed for the theory while focusing on improving the kinetics. For this an analysis of the mean first passage times (MFPTs) required for detailed molecular evaporation/condensation growth steps to reach and exceed the critical cluster (consisting of seed particle plus condensate) size is presented. Recent results from Wedekind et al. [2007] are extended for this purpose to the kinetics of heterogeneous nucleation. Series expansions for MFPT and nucleation rate are evaluated numerically and used to derive a simple analytic expression for predicting heterogeneous nucleation rate. Comparison with the full MFPT calculation shows the approximate formula to be accurate to within a few percent for nucleation barrier heights in excess of about 5 kT – a range well covering the region of interest to the present study.

Although physical and chemical properties are derived from the capillarity approximation, an new approach to the thermodynamic analysis is presented. As described in Sec. 2, the approach is based on graphical constructions derived from the Kelvin curve. There are several reasons for pursuing the new approach: It provides convenient area constructions for homogeneous and heterogeneous nucleation barriers and a graphical interpretation even for key kinetic terms, such as the Zeldovich factor, used in the newly derived rate expression. The method further simplifies the scaling analysis used to correlate working fluid performance in Sec. 5. Finally the graphical approach provides a molecular-based framework that recovers results from classical nucleation theory when the capillarity approximation is used but unlike the conventional derivation lends itself to a molecular description that can incorporate departures from the classical theory.

The new results are discussed in the context of early speculations on the application of nucleation and growth as a detection tool for single neutral molecules and clusters [Reiss et al., 1977]. A full analysis of detection capability will require, among other considerations, going beyond Fletcher theory and viewing heterogeneous nucleation as a multi-component molecular interaction process in the nano regime. Here we take preliminary steps in this direction to show that the new formulation provides a molecular level framework, rooted in mass action and detailed balance, which can be exploited to great advantage in attempts to go beyond classical nucleation theory.

2. Thermodynamic area constructions

This section develops several graphical constructions for key thermodynamic properties that include nucleation barrier height, surface work, and barrier shape. The approach derives from the Kelvin relation, which gives the critical size (generally consisting of seed plus condensed fluid) as a function of vapor saturation ratio:

$$\ln\left(\frac{P_{eq}(g)}{P_{eq}^{\infty}}\right)=\left(\frac{32\pi}{3}\right)^{1/3}\left(\frac{\sigma v_1^{2/3}}{kT}\right)g^{-1/3}. \qquad (2.1)$$

Here $g = n_{seed} + n$ is the number of condensed solvent molecules, each of molecular volume v_1, required to fill the total volume, v, consisting of the seed particle volume, $v_{seed} \equiv n_{seed} v_1$, plus condensate, $v_{cond} = n v_1$. Equivalently, g is the number of liquid-phase condensate molecules present in the same-size homogeneous drop, $v = g v_1$. Note that n_{seed} refers not to the number of molecules actually present in the seed, but to a volume-equivalent number expressed here as the number of molecules of the condensed working fluid required to fill the volume occupied by the seed. $P_{eq}(g)$ is the vapor pressure in (unstable) equilibrium with the drop and P_{eq}^{∞} is the bulk equilibrium vapor pressure over a

flat surface. The non-dimensional group of physical constants appearing on the right hand of Eq. 2.1, which will henceforth be written as $\Omega / T \equiv \sigma v_1^{2/3} / kT$, is a convenient scaling parameter used extensively in the sequel. Here σ is bulk surface tension, v_1 is derived from the bulk density, and $\Omega = \sigma v_1^{2/3} / k$ has units of temperature.

Barrier profiles for both heterogeneous and homogeneous nucleation may be derived using thermodynamic area constructions similar to those introduced recently to analyze the deliquescence and efflorescence of small particles [McGraw and Lewis, 2009]. The fundamental equation takes the following form:

$$\frac{W(n)}{kT} = \int_0^n \ln\left(\frac{P_{eq}(n')}{P_{ext}}\right) dn' \tag{2.2}$$

where n is the actual (not volume equivalent) number of condensed solvent molecules present in the particle, n' is a dummy integration variable and $W(n)$ is the reversible work required to condense n molecules from the surrounding external vapor at pressure P_{ext}. Derivation of Eq. 2.2 from the molecular-level kinetics of cluster evaporation and growth using only the law of mass action and principle of detailed balance is given elsewhere [McGraw and Lewis, 2009], but its content is motivated here for the special case of classical homogeneous nucleation theory. The homogeneous nucleation barrier profile is recovered for $n_{seed} = 0$, in which case $n = g$. Then a similar equation to Eq. 2.2 but with P_{eq}^{∞} replacing P_{ext}, in which case the integrand is simply the logarithm of the saturation ratio along the Kelvin curve, gives the reversible work required to extrude a drop from bulk liquid under *saturated* conditions – equal to the surface tension times the surface area, $A(n)$, of the drop [Reiss, 1996]. The difference, $-n \ln\left(P_{ext} / P_{eq}^{\infty}\right) = -n \ln S_{ext}$, where S_{ext} is the saturation ratio, is the reduced work gained by condensing n molecules

of the (supersaturated) external vapor to bulk liquid prior to starting the extrusion process. Adding these two contributions gives $W(n) = -n \ln S_{ext} + A(n)\sigma$, showing that for this special case Eq. 2.2 yields the classical result.

Figure 1 illustrates area constructions for both homogeneous and heterogeneous nucleation using water vapor at 200% relative humidity (RH) as an example. For the homogeneous case the reduced barrier height is:

$$\frac{W^*_{homo}}{kT} = A_1 + A_2, \tag{2.3}$$

which follows from Eq. 2.2 for the upper limit of integration set at $n = n^* = g^*$, the intersection of the Kelvin curve (solid curve) and horizontal dashed line. The sub-areas, also defined with respect to the Kelvin curve, are indicated in the figure and labeled with a subscript to distinguish them from surface area. In the heterogeneous case, for seed volume v_{seed}, the integration in Eq. 2.1 is from $n' = 0$ ($g = v_{seed}/v_1$) to n^* ($g = g^*$), yielding the reduced barrier height

$$\frac{W^*_{hetero}}{kT} = A_1. \tag{2.4}$$

A conceptual advantage of the new approach is that, in principle, it avoids the un-natural separation into surface and bulk properties inherent in the capillarity drop model. Thus if the true vapor pressure curve P_{eq} were somehow available, e.g. from a molecular simulation of cluster evaporation rate, Eq. 2.2 would remain valid – the only requirements being an ideal vapor mixture (an excellent approximation at near atmospheric pressure conditions) and cluster condensation and evaporation rates that satisfy detailed balance [McGraw and Lewis, 2009]. In absence of a sufficiently accurate molecular-based approach we continue with the capillarity approximation, in which case

the barriers from graphical construction reduce exactly to those derived conventionally from classical nucleation theory.

Several well-known, capillarity-based, relations for the barrier height follow easily from the graphical construction when the vapor pressure is given by the Kelvin relation. Continuing with the homogeneous case we obtain the two equivalent results:

$$\frac{W^*_{homo}}{kT} = \frac{1}{2} g^* \ln\left(\frac{P_{ext}}{P^\infty_{eq}}\right) = \frac{1}{2}(A_3 + A_4). \tag{2.5a}$$

$$\frac{W^*_{homo}}{kT} = \frac{1}{3}\frac{A^*\sigma}{kT} = \frac{1}{3}(A_1 + A_2 + A_3 + A_4) \tag{2.5b}$$

where $A^* \equiv A(g^*)$ is the surface area of the critical cluster. Equation 2.5a is important to the scaling analysis of Sec. 5. The first equality of Eq. 2.5b can be traced to the work of Gibbs [Gibbs, 1906]. The first area equality (Eq. 2.5a) follows trivially from the figure; the second (Eq. 2.5b) follows the previous discussion of droplet extrusion. Full barrier profiles for either heterogeneous or homogeneous ($n_{seed} = 0$) nucleation follow from Eq. 2.2 with limits of integration from n_{seed} to $n_{seed} + n$ for variable *n*, where *n* is the number of molecules of liquid condensate:

$$\frac{W(n)}{kT} = A_1(n) = -n\ln\left(\frac{P_{ext}}{P^\infty_{eq}}\right) + (36\pi)^{1/3}\left(\frac{\Omega}{T}\right)[(n_{seed} + n)^{2/3} - n^{2/3}_{seed}), \tag{2.6}$$

in agreement with the classical result. Ω / T is the previously defined physical constant grouping appearing in parenthesis on the right hand side of Eq. 2.1. The function $A_1(n)$ evaluated at the critical size $n = n^*$ equals A_1. Dividing the first and second terms on the right hand side of Eq. 2.6 by the middle terms from Eqs. 2.5a and 2.5b, respectively, gives the following working-fluid-independent result:

$$\frac{W(n)}{W^*_{homo}} = 3\left(\frac{n}{g^*} + f\right)^{2/3} - 2\left(\frac{n}{g^*} + f\right) - (3f^{2/3} - 2f) \qquad (2.7)$$

where $f = v_{seed}/(g^* v_1) = n_{seed}/g^*$ is the ratio of seed volume to volume of the critical particle. At the critical condition

$$\frac{W^*}{W^*_{homo}} = \frac{A_1}{A_1 + A_2} = -3f^{2/3} + 2f + 1. \qquad (2.8)$$

The homogeneous ($f = 0$) limit of Eq. 2.7 was utilized previously [McGraw, 2001]. Here the more general result shows that the barrier profiles for perfect wetting are characterized by a universal one-parameter family of curves independent of the detailed physio-chemical properties of the condensing fluid. These curves are shown in Fig. 2 for several values of *f*.

For use in the following section we require the Zeldovich factor, which is a measure of barrier curvature at the critical size [Abraham, 1974]:

$$Z = \sqrt{\frac{-1}{2\pi}\left[\frac{\partial^2 (W^*_{homo}/kT)}{\partial g^2}\right]_{g^*}} = \sqrt{\frac{-1}{2\pi}\left[\frac{\partial^2 (W^*_{hetero}/kT)}{\partial n^2}\right]_{n^*}} = \sqrt{\frac{-\gamma}{2\pi}} \qquad (2.9)$$

The first equality is the definition of this quantity. The second equality shows that Z has the same value for the homogeneous nucleation and perfect wetting heterogeneous nucleation cases. This follows by inspection of the graphical construction and provides an interpretation for the second partial derivatives as each equal to the slope, γ, of the Kelvin curve at g^* (Fig.1). That the same Zeldovich factor applies in the two cases is seen graphically as a simple consequence of the slopes being the same. Vehkamäki et al. [2007] provide a convenient formula for evaluating Z for heterogeneous nucleation on spherical particles under more general nonzero contact angle conditions. Using their results we have shown (unpublished) that the same area and slope constructions for

W^*_{hetero}/kT and Z, respectively, apply as well in the more general case. Of course $P_{eq}(n)$ depends on contact angle and only (discontinuously) reduces to the Kelvin curve for perfect wetting. Evaluating the slope of the Kelvin curve gives:

$$Z = \sqrt{\frac{1}{6\pi}\frac{\ln S_{ext}}{g^*}} = \frac{1}{8\pi}\left(\frac{\Omega}{T}\right)^{-3/2}(\ln S_{ext})^2 \qquad (2.10)$$

where in the second equality g^* has been eliminated in favor of $\ln S_{ext} \equiv \ln(P_{ext}/P^{\infty}_{eq})$.

3. Mean first passage time (MFPT) kinetics and activation rate

Consider a collection of condensate free ($n = 0$) seed particles, M, of initial vapor phase concentration $[M]_0 = N_0$, uniform diameter d_{seed}, and zero contact angle for wetting by the working fluid. The subsequent uptake and exchange of molecules from the working fluid, presence in the supersaturated vapor at concentration $[F_1] = n_v$, is described by the following sequence of condensation/evaporation steps:

$$\begin{aligned} M + F_1 &\leftrightarrow MF_1 \\ MF_1 + F_1 &\leftrightarrow MF_2 \\ &\vdots \\ MF_n + F_1 &\leftrightarrow MF_{n+1} \end{aligned} \quad . \qquad (3.1)$$

A similar kinetics applies to homogeneous nucleation on replacement of M by F_1. Particles sufficiently large (e.g. twice the critical cluster size MF_{n^*}) are assumed far enough into the growth-dominated regime so as to no longer be able to re-cross the barrier to their pre-critical state at any reasonable rate. This is essentially the same argument used to introduce the Szilard absorbing boundary condition in classical nucleation theory [Abraham, 1974] and for the present application justifies the placement of an imaginary model boundary distinguishing “un-activated” from “activated” particles. Because the boundary is in effect absorbing (no-returns) the model activation rate equals

the rate of first crossing, and the per particle activation rate (see below) equals the reciprocal of the mean first passage time (MFPT), also defined below (see Eq. 3.5).

Model assumptions: We use an exponential decay kinetics that has previously been applied to activation in supplementary online material by Winkler et al. [2008]:

$$\frac{dN}{dt} = -J_{hetero} = -J_1 N. \tag{3.2}$$

In the last equality particles are treated as independent to the extent that the steady state nucleation rate, J_{hetero} (number of particles activated per unit volume per second), is proportional to the number concentration of remaining un-activated particles, N:

$$J_{hetero} = NJ_1 \tag{3.3}$$

where J_1 is the per-particle crossing rate. During a short time interval dt, $J_{hetero}dt$ particles per unit volume are lost to activation. Combining these results gives

$$N(t) = N(0)e^{-J_1 t} \tag{3.4}$$

where $N(0)$ is the initial number concentration of seed particles and the exponent gives the probability that any given particle remains un-activated at time *t*. Several assumptions are implicit in the model that a direct calculation of the MPFT and comparison with measurement can test. First, the assumption of steady state nucleation rate: Conditions under which the quasi equilibration of pre-critical clusters and steady state nucleation are reached on timescales short compared with the decay of N are evident in a calculation of the MPFT as a function of boundary location. Second, the exponential decay model requires random rather than deterministic activation – a property that can also be checked through a study of the MPFT. Finally Eq. 3.2 assumes that just one seed particle is present in the critical nucleus. This is easily tested experimentally using the nucleation theorem (Eq. 4.13) below.

Calculation of the mean first passage time: We classify un-activated (activated) particles as those belonging to size class MF_{nmax} and smaller (MF_{nmax+1} and larger) where $nmax = 2n^*$. Interest is primarily in the MFPT to reach MF_{nmax+1} so defined, but a study for variable *nmax*, to show insensitivity to boundary placement at $2n^*$ and verify other assumptions implicit in the exponential model, was also carried out. Let U be the domain of un-activated particles such that $MF_n \in U$ for $0 \le n \le nmax$ and let $P_U(t)$ be the probability that a seed that is condensate-free at $t = 0$ remains in the un-activated domain at time *t*. Then the fraction of particles *leaving U* at time *t* is $-dP_U(t)/dt$. By definition, the MFPT is the mean time it takes to leave *U*, which is [Hänggi, et al., 1990]:

$$\tau \equiv -\int_0^\infty t \frac{dP_U}{dt} dt = \int_0^\infty P_U(t) dt . \qquad (3.5)$$

The last equality follows an integration by parts. Evaluating the last integral for the exponential decay model gives $\tau = 1/J_1$.

Benchmark calculations are based on the following formula for the MFPT [Hänggi et al., 1990; Wedekind et al., 2007]:

$$\tau(nmax) = \sum_{j=0}^{nmax} \left(\frac{e^{W_{hetero}(j)/kT}}{D_j} \sum_{i=0}^{j} e^{-W_{hetero}(i)/kT} \right). \qquad (3.6)$$

The double summation is a discretized version of Eq. 2 of Wedekind et al. [2007]. Dummy indices i and j refer to the number of condensate molecules in the seed-condensate particle (the n in MF_n) and the summation begins with the initial seed, M ($n = 0$). Equation 3.6 describes the case of particles undergoing diffusion-drift along the size coordinate, *n*, with reflecting and absorbing boundaries located at 0 and $nmax + 1$, respectively. D_j is the size-dependent diffusion coefficient along the growth coordinate,

which is also equal to the collision rate of vapor molecules with a particle of size $n = j$ ($g = n_{seed} + j$) (McGraw, 2001):

$$D_j = n_v \sqrt{\frac{8\pi kT}{m_v}} r_1^2 (n_{seed} + j)^{2/3} = \frac{P_{ext} A(j)}{\sqrt{2\pi m_v kT}}. \qquad (3.7)$$

Here r_1 is the vapor monomer radius corresponding to the molecular volume v_1, n_v is the vapor number concentration, m_v is vapor molecular mass, and $A(j) = 4\pi r_1^2 (n_{seed} + j)^{2/3}$ is the surface area of the seed-condensate cluster for $n = j$. Direct evaluation of the double summation of Eq. 3.6 provides the benchmark against which a new approximate formulation for J_1 will be tested and used to analyze the scaling properties of heterogeneous particle activation rate in the following section.

4. A simple but accurate expression for mean first passage time and heterogeneous nucleation rate

Figure 3 illustrates a typical distribution of the MFPTs required to exceed any specified (seed plus condensate) particle size as a function of that size or, equivalently, as a function of the upper limit, $nmax$, in the double summation of Eq. 3.6. The steep inflection region centered at the critical size (region II) is indicative of wide separation of time scales between the rapid quasi-equilibration of pre-critical particles (region I) and the significantly slower barrier crossing. The figure also shows the MFPT to be insensitive to *nmax* sufficiently beyond the critical particle size (region III). Henceforth we set $nmax = 2n^*$. In addition to separation along the time coordinate, there is a distinct separation with respect to particle size: The overwhelming majority of rapidly equilibrated pre-critical clusters tend to be significantly smaller than the critical particle size and dominate the summation over i. On the other hand the summation over j is

dominated by terms near the critical size. Accordingly, to good approximation the double summation factors into to a product of two single-index summations. Specifically, the size separation allows one to choose a value, $imax$, such that terms in the inner summation having $i > imax$ may be neglected even though $imax$ is still significantly smaller than the critical size. Meanwhile the critical size so dominates the summation over j that terms in the outer summation having $j \le imax$ may be neglected. Modifying the ranges of the two indices to cover only non-neglected terms gives the expression to the right of the approximate equality, below, and the factorization:

$$\tau(2n^*) = \frac{1}{J_1} \approx \sum_{j=imax+1}^{2n^*} \left(\frac{e^{W_{hetero}(j)/kT}}{D_j} \sum_{i=0}^{imax} e^{-W_{hetero}(i)/kT} \right) = \sum_{j=imax+1}^{2n^*} \frac{e^{W_{hetero}(j)/kT}}{D_j} \sum_{i=0}^{imax} e^{-W_{hetero}(i)/kT} \quad (4.1)$$

A series of further approximations is now made to the factored expression: First D_j is approximated by its value at the critical size

$$D_j \approx D_{j^*} = n_v \sqrt{\frac{8\pi kT}{m_v}} r_1^2 (n_{seed} + j^*)^{2/3} = \frac{P_{ext} A(j^*)}{\sqrt{2\pi m_v kT}} \quad (4.2)$$

and factored out of the summation. Second, the remaining part of the summation over j is approximated in the usual manner of nucleation theory by its maximum term multiplied by the correction factor of Zeldovich to yield the intermediate result:

$$\tau(2n^*) = \frac{1}{J_1} \approx \frac{1}{D_{j^*}} \frac{1}{Z} e^{W_{hetero}(j^*)/kT} \sum_{i=0}^{imax} e^{-W_{hetero}(i)/kT} . \quad (4.3)$$

The i^{th} term of the last summation is a Boltzmann factor proportional to the quasi-equilibrium number concentration of seed-condensate particles of size $n = i$. Thus the

total number concentration of pre-critical particles is proportional to the summation itself. Linearization of the reduced work about $i = 0$ gives

$$W_{hetero}(i)/kT \approx hi \tag{4.4}$$

with slope:

$$h = \left(\frac{32\pi}{3}\right)^{1/3} \frac{\Omega}{T}(n_{seed})^{-1/3} - \ln\left(\frac{P_{ext}}{P_{eq}^{\infty}}\right) = \ln S_{ext}\left(f^{-1/3} - 1\right) \tag{4.5}$$

wherein the first term on the right hand side derives from Eq. 2.1. Apart from a dimensionless scaling factor $W_{homo}^{*}/g^{*}kT = \ln S_{ext}/2$ (Eq. 2.5), h is the initial slope of the scaled, *f*-dependent barrier height shown in Fig. 2. Geometrically, h is the length of the solid vertical line segment separating regions A_1 and A_2 in Fig. 1. This ranges from a very large value in the homogeneous nucleation limit ($n_{seed} = 0;\ n = 1$) to zero at the critical size. Under the assumed condition that a suitable *imax* can be chosen such that the quasi-equilibrium number concentration of particles beyond MF_{imax} is a negligible fraction of the initial seed concentration, the summation appearing on the right hand side of Eq. 4.3 can be further approximated as:

$$\sum_{i=0}^{imax} e^{-W_{hetero}(i)/kT} \approx \sum_{i=0}^{imax} e^{-hi} \approx \sum_{i=0}^{\infty} e^{-hi} = \frac{1}{1-e^{-h}} \tag{4.6}$$

where in the first approximate equality Eq. 4.4 has been used. Substitution into Eq. 4.3 gives our final form for the per-seed heterogeneous nucleation rate (units s^{-1})

$$J_1 = \frac{1}{\tau} \approx \frac{P_{ext}A(j^{*})}{\sqrt{2\pi m_v kT}}(1-e^{-h})Ze^{-W_{hetero}^{*}/kT}, \tag{4.7}$$

and

$$J_{hetero} \approx N\frac{P_{ext}A(j^{*})}{\sqrt{2\pi m_v kT}}(1-e^{-h})Ze^{-W_{hetero}^{*}/kT} \tag{4.8}$$

for the total heterogeneous nucleation rate.

Equations 3.1 describe an associating vapor. For large slope (h) the distribution of precritical seed-condensate clusters is dominated by the $n = 0$ condensate-free seeds, M and $[M] = N$. For the general case that association is present $[M] = (1 - e^{-h})N$ and Eq. 4.8 becomes:

$$J_{hetero} \approx [M] \frac{P_{ext} A(j^*)}{\sqrt{2\pi m_v kT}} Z e^{-W^*_{hetero}/kT} \qquad (4.9)$$

which is proportional to the concentration of the starting species – seeds without condensate. The concentration of condensate-free seeds $[M]$, treated here as just another molecular constituent of the vapor, is reduced below N by the association factor $1 - e^{-h}$, and J_{hetero} is correspondingly reduced. This is an example of the somewhat counterintuitive effect that association has on increasing the stability of a metastable vapor phase by suppression of the nucleation rate (Katz et al., 1966).

Homogeneous nucleation rate: At high enough saturation ratio, homogeneous nucleation of the vapor itself will compete with heterogeneous nucleation and interfere with particle detection - making the comparison of these two nucleation channels a necessary consideration. The homogeneous nucleation rate is [Abraham, 1974]:

$$J_{homo} = n_v \left(\frac{P^\infty_{eq}}{P_{ext}} \right) \frac{P_{ext} A(g^*)}{\sqrt{2\pi m_v kT}} Z e^{-W^*_{homo}/kT} = n_v^{eq} \frac{P_{ext} A(g^*)}{\sqrt{2\pi m_v kT}} Z e^{-W^*_{homo}/kT}. \qquad (4.10)$$

As noted previously, Z has the same value here as in the heterogeneous case. The vapor pressure ratio in parenthesis to the right of the first equality supplies the $1/S_{ext}$ correction due to Courtney (1961). It should be noted that Courtney's correction, which derives from the addition of a term $kT \ln(P_{ext}/P^\infty_{eq})$ to the classical W_{homo} in order to gain

consistency with the law of mass action, does not apply to W_{hetero} because the correction cancels on taking free-energy differences relative to M when a seed is present. On shift from negative exponent to kinetic prefactor, the Courtney correction amounts to the additional factor of $1/S_{ext}$ appearing in Eq. 4.10 for the homogeneous nucleation rate.

Testing the new rate expression: Figures 4 and 5 show the Kelvin curve together with the calculated homogeneous nucleation threshold range from Eq. 4.10 (here shown for rates within ± 2 orders of magnitude of $J_{homo} = 1\ cm^{-3}s^{-1}$) and heterogeneous nucleation threshold range from Eq. 4.7 (rates within ± 2 orders of magnitude of $J_1 = 1s^{-1}$). The filled circles are from the full double summation for the MFPT for $\tau = 1s$ (Eq. 3.6 with $nmax = 2n^*$) and should be compared with the approximate expression (middle curve) for $J_1 = 1s^{-1}$. Agreement is excellent: to within about 5% in the case of menthol and 2% for water. The larger discrepancy for menthol is probably due to discretization error as the number of molecules in the critical nucleus is considerable smaller than in the case of water. Barrier heights are in the range $10 - 20kT$; much lower than for homogeneous nucleation where typical barrier heights range between 50 and 70 kT (see below). Closer to the Kelvin limit, e.g. for barrier heights lower than about 5 kT, the approximations used to derive the new analytic expression begin to fail and the full double summation formula for the MFPT should be used instead. The exponential decay model (Eq. 3.4) will also fail in this regime as activation begins to take on less the character of a random barrier crossing process and more one of deterministic growth. According to the 5 kT criterion the simplified expression for heterogeneous nucleation rate can be used reliably for $f \leq 0.5$ (or d_{seed}/d_{Kelvin} less than about 80%). This is the predominant range of interest anyway as the general goal is to achieve selective detection

of the smallest particles, which is favored by being close to the heterogeneous nucleation threshold and well below the Kelvin limit. For $f \leq 0.5$ the association factor is typically between 0.2 and 1 while $1/S_{ext}$ typically exceeds 0.01. In the context of nucleation such corrections are oftentimes regarded as small but here they are needed to achieve the few percent level of accuracy with reference to the MFPT benchmark we have described.

Nucleation theorems: Nucleation theorems give the relative sensitivity of nucleation rate to saturation ratio, temperature, or other constraint [Kashchiev, 1982; McGraw and Wu, 2003]. The following relations in terms of the log saturation ratio follow immediately from the area construction (Fig. 1) on application of the fundamental theorem of integral calculus to the areas A_1 and $A_1 + A_2$:

$$\frac{\partial \ln J_{hetero}}{\partial \ln S_{ext}} = \frac{\partial \ln K_{hetero}}{\partial \ln S_{ext}} - \frac{\partial W^*_{hetero}/kT}{\partial \ln S_{ext}} = 1 - \frac{\partial(A_1)}{\partial \ln S_{ext}} = 1 + g^* - n_{seed} = 1 + n^* \quad (4.11)$$

$$\frac{\partial \ln J_{homo}}{\partial \ln S_{ext}} = \frac{\partial \ln K_{homo}}{\partial \ln S_{ext}} - \frac{\partial W^*_{homo}/kT}{\partial \ln S_{ext}} = 1 - \frac{\partial(A_1 + A_2)}{\partial \ln S_{ext}} = 1 + g^*. \quad (4.12)$$

Partial derivatives are taken at constant temperature and K_{hetero} and K_{homo} are the prefactors from Eqs. 4.8 and 4.10, respectively, for the heterogeneous and homogeneous nucleation rate, each of which makes a contribution of unity to the relative sensitivity. Evaluating instead the relative sensitivity with respect to seed concentration gives:

$$\frac{\partial \ln J_{hetero}}{\partial \ln N} = 1 \quad (4.13)$$

as expected from the one-seed-per-critical-nucleus assumption. More generally, measurement of $\partial \ln J_{hetero} / \partial \ln N$ yields the number of seed particles present in the critical nucleus. Another heterogeneous nucleation theorem that follows immediately

from inspection of the area construction gives sensitivity of the log rate to changes in seed particle size, n_{seed}:

$$\frac{\partial \ln J_{hetero}}{\partial n_{seed}} \approx -\frac{\partial A_1}{\partial n_{seed}} = h \qquad (h \geq 0). \qquad (4.14)$$

The approximate equality neglects a small contribution from the association term in the kinetic prefactor. The requirement that *h* be non-negative is discussed in Sec. 6.

5. Fundamental limits to neutral particle detection

Maximizing detector sensitivity: Avoiding interference from homogeneous nucleation requires that the homogeneous nucleation rate be less than or comparable to the activation rate: $J_{homo} / J_{hetero} \leq 1$ or, from Eq. 3.3, $J_{homo} / J_1 \leq N(cm^{-3})$. Under typical CPC measuring conditions N is the 10-1000 cm^{-3} range. Nucleation thresholds are typically sharp, as illustrated for menthol and water in Figs. 4 and 5. The figures show threshold bands, where the rates $J_{homo}\,(cm^{-3}s^{-1})$ and $J_1\ (s^{-1})$ take on mid and extreme values of 1, 10^{-2}, and 10^{2}, and characteristically small intersection regions where the ratio J_{homo} / J_1 ranges from 10^{-4} to 10^{4}. Operation near the homogeneous nucleation threshold, $J_{homo} = 1\ (cm^{-3}s^{-1})$, which condition defines the critical saturation ratio S_{cr}, maximizes detector sensitivity. The smallest particles will be detected under conditions that are also close to the heterogeneous nucleation threshold, $J_{hetero} = 1\ (cm^{-3}s^{-1})$ where the above inequalities are satisfied but not overly so. These conditions are now used to establish fundamental size and concentration limits to neutral particle detection.

Signal to noise ratio perspective: Taking nucleation rates from Eqs. 4.8 and 4.10, the preceding criterion becomes:

$$\frac{J_{homo}}{J_{hetero}} = \frac{n_v^{eq}}{N}\left(\frac{1}{1-e^{-h}}\right)\frac{A(g^*)}{A(n^*)}e^{-(W^*_{homo}-W^*_{hetero})/kT} = \frac{n_v^{eq}}{N}\left\{\left(\frac{1}{1-e^{-h}}\right)e^{-A_2}\right\}$$

$$\approx \frac{n_v^{eq}}{N}e^{-A_2} = \frac{n_v^{eq}}{N}Exp\left[-\frac{W^*_{homo}}{kT}\left(3f^{2/3}-2f\right)\right] \le 1. \qquad (5.1)$$

The second equality uses the fact that the surface area ratio is unity. As before $f = n_{seed}/g^*$ and A_2, the area under the Kelvin curve referenced in Fig. 1, has been evaluated in the last equality using Eq. 2.8. In the approximate equality we neglect the inverse association factor, which as noted previously is typically close to unity and much less important to the subsequent discussion than n_v^{eq}, A_2, or N. The expression to the right of the approximate equality has an especially transparent interpretation in terms of signal to noise ratio: For steady state homogeneous nucleation the constrained equilibrium concentration of clusters of size n_{seed} is given by $n_v^{eq}e^{-A_2}$, where A_2 is the reversible work required to assemble a pre-critical cluster of this size from vapor in the capillary drop model. (That the concentration of vapor in equilibrium with bulk liquid n_v^{eq} appears, rather than the actual supersaturated vapor concentration n_v, follows Courtney [1961]). Although these precritical clusters arise from thermal fluctuations in the vapor, they have the same probability to subsequently grow to critical size and contribute to homogeneous nucleation rate that the permanent perfect wetting seeds have of contributing to heterogeneous nucleation rate. Whenever the two concentrations are equal, the homogeneous and heterogeneous nucleation rates will also be the same. The expression to the right of the approximate equality is simply this ratio of concentrations: fluctuating clusters of seed size (thermal noise) to actual seeds N (signal). Viewed from this perspective the ratio $n_v^{eq}e^{-A_2}/N$ should normally be maintained less than unity, and

its inverse, the signal to noise ratio (SNR), greater than unity in order that the concentration of homogeneously formed clusters not exceed the concentration of seeds. (One can conceive of tricks to work with lower SNRs, like modulating the seed concentration, but such considerations are beyond the scope of the present study). Figure 6 shows curves of constant $\mathrm{SNR} = 1$ (equivalently curves for which $N = n_v^{eq} e^{-A_2}$) for *n*-butanol at two different temperatures and three different nucleation rates obtained by varying S_{ext}. Detection at smaller size is seen to be favored by higher N, lower T, and lower S_{ext}.

Scaling and minimum detection size: Because the working fluid enters only through its equilibrium vapor pressure and non-dimensional *homogeneous* nucleation parameters, corresponding states scaling ideas previously developed to correlate the homogeneous nucleation thresholds of supersaturated vapors [McGraw, 1981; Rasmussen and Babu, 1984; Hale, 1992] can be used here. The power of scaling is illustrated through its application to a selection of four widely different working fluids for which homogeneous nucleation measurements are available (Fig. 7 and Table 1). Each of the material-characteristic points in Fig. 7 lies at the intersection of several important curves: the hyperbola of constant homogeneous nucleation barrier height (Eq. 2.5a), the Kelvin curve, which depends on the scaling parameter Ω / T, and the horizontal and vertical lines marking $\ln S_{cr}$ and g^*, respectively. To avoid crowding the figure, while sufficing to illustrate the method, the full set of intersecting curves is drawn only for nonane. The parameters needed to construct similar curves for each of the other materials are provided in the table. Homogeneous nucleation barrier heights for many substances tend to be in

the $50kT - 70kT$ range bounded by the dashed hyperbolic curves [McGraw, 1981], as illustrated in the figure.

The maximum sensitivity condition for each working fluid lies close to the critical saturation ratio, indicated in Fig. 7 for nonane by the horizontal dotted line. The threshold values of first row of Table 1 were obtained from Eq. 4.10 by adjusting S_{ext} to have $J_{homo} = 1$. Thus the minimum detection size lies close to the $\ln(S_{cr})$ line, between 0 and g^*, and close to the heterogeneous nucleation threshold. Its location is obtained by solving the equality limit of Eq. 5.1 (here with seed concentration $N = 1\ cm^{-3}$) for $f^{min} \equiv n_{seed}^{min} / g^*$. The result is marked by the caret in Fig. 7 for nonane and provided for the other materials in row 7 of the table. Near constancy of this ratio for the different working fluids suggests its value as an important *heterogeneous* nucleation scaling parameter. Using molecular volumes, obtained from the bulk liquid density (row 10), to covert n_{seed}^{min} to a spherical mass-equivalent volume gives the minimum detectable seed particle diameters shown in the last row of the table. The entries for menthol and water match particle diameters near the centers of the threshold intersection regions shown in Figs. 4 and 5. The smallest diameter of the set, at $1.14\,nm$, is found for water even though its scaling parameters are very close to those of *n*-butanol at 300K, which has the second highest minimum detection diameter at $1.96\ nm$. The molecular based n_{seed}^{min} values are close for water and *n*-butanol, so the main difference lies in the significantly smaller molecular volume of water. Comparing water and menthol we see that the latter has the highest Ω / T (row 3), which gives it the smallest g^* (row 4). Here again water wins out for having the smaller detection diameter due to its factor of eight smaller molecular volume.

The scaling parameter Ω/T contains T implicitly in Ω and explicitly in $1/T$. A useful approximate form for the temperature dependence of Ω/T has been obtained by Hale [1992] for surface tensions approximated by a linear form, $\sigma = \sigma_0(T_c - T)$, where T_c is the critical temperature. Neglecting a small temperature dependence in density gives $\Omega/T \approx \Omega_H(T_c/T - 1)$, with $\Omega_H \equiv \sigma_0 v_1^{2/3}/k$. Temperatures dependence is exhibited in Fig. 7 for the case of *n*-butanol at 10-degree intervals from 250 to 320 *K* by the triangles positioned from left to right, respectively.

Nucleation and growth as a detection tool: The preceding discussion examined the case that $N \approx 1\ cm^{-3}$ and applies to the detection of seed particles (or large molecular impurities) of volume $n_{seed}^{min} v_1$ present in the vapor at concentrations of order $1\ cm^{-3}$. The question naturally arises as to whether or not it is possible to detect still smaller particles and even single neutral molecules this way. According to Eq. 5.1, and Fig. 6, the detection of molecule "impurities" comparable in size to the molecular volume of the working fluid requires their presence at the much higher concentration $N \approx n_v^{eq}$. Intermediate sizes require intermediate seed concentrations N (Fig. 6). Efficiency of particle detection is defined as:

$$\varepsilon = 1 - \frac{N(\tau)}{N(0)} = 1 - e^{-J_1 \tau} \qquad (5.2)$$

where $N(\tau)$ is the concentration of unactivated particles leaving the CPC after residence time τ. A typical CPC residence time of $\tau = 0.1s$, and $J_1 = 1\ cm^{-3}s^{-1}$, gives $\varepsilon = 0.1$, which is the detection efficiency at the minimum detectable particle sizes reported in Table 1. Efficiency is a metric that doesn't include noise and ε will vary widely along the $SNR = 1$ curves of Fig. 6. Thus, having $N = 100\ cm^{-3}$ gives a noticeably smaller

detection limit than having $N = 1$ at the same *SNR*. For comparable residence times, the smaller particles will be detectable at only 1% of the efficiency for detection at the size limits reported in Table 1, which are all based on having $N = 1\ cm^{-3}$.

Evidence for the detection of critical nuclei containing just one organic molecule comes from laboratory measurements on the ternary p-toluic acid/sulfuric acid/water [Zhang et al., 2004] and cis-pinonic acid/sulfuric acid/water [Zhang et al., 2009] systems and their interpretation using the nucleation theorem [McGraw and Zhang, 2008]. In both cases the concentration of the organic acid present in the vapor was of order $10^{10}\ cm^{-3}$- far in excess of unity, and comparable to the sulfuric acid vapor concentration. For a nucleation rate of $10^{3} cm^{-3} s^{-1}$ this implies a detection frequency for the organic acid in the 10^{-8} range. Noise arises due to binary homogeneous nucleation in the background sulfuric acid/water vapor mixture. Analysis of ternary to binary nucleation rate ratios in the *p*-toluic acid/sulfuric acid/water system [Fig. 4 of McGraw and Zhang, 2008] gives SNRs for detection of *p*-toluic acid in the 5-10 range.

In their investigations of nucleation and growth as a detection tool Reiss et al. [1977] conclude, " it is unlikely, however, that single neutral molecules can be detected [referring to detection using a diffusion cloud chamber], although the possibility remains for detecting individual polymer molecules of a substantial degree of polymerization". Elsewhere in their paper these authors state, "even though theory shows that one cannot *detect* a single impurity molecule, it shows that there may be cases in which a nucleus contains only a single [such] molecule. But this is not the same as having *every* impurity molecule serve as a nucleus". These findings are consistent with the results obtained here. The following section presents a preliminary analysis showing that the graphical method

can be used to incorporate departures from the Kelvin relation from interactions at the molecular scale.

6. Incorporating departure from the Kelvin relation

An important tool for direct testing of the Kelvin relation for small droplets became available with the ability to measure nucleation rates (as opposed to earlier measurements that yielded only nucleation threshold conditions). Strey et al. [1994] performed such a test using homogeneous nucleation rate measurements in conjunction with the nucleation theorem to give a determination of critical cluster size for *n*-butanol. The Kelvin relation sufficed to predict cluster sizes down to as few as 40 molecules an equivalent radius of curvature of 1 nm. Similar studies for water showed agreement down to about 30 molecules or about 0.6 nm radius of curvature [Wölk and Strey, 2001]. One concludes from these studies that even though the Kelvin relation relies on macroscopic surface tension and density to predict the vapor pressures of small drops, it tends to work surprisingly well.

A seemingly common case in homogeneous nucleation occurs when the Kelvin relation works well for clusters of critical size but fails for smaller ones. This situation is depicted schematically in Fig. 8 by the dotted vapor pressure curve $[P = P_1(g)]$ for the case of attractive interactions that lower the vapor pressures of very small clusters relative to the Kelvin curve. The integrated area between $P_1(g)$ and the dashed line at $\ln S_{ext}$ equals the corrected reduced barrier height for homogeneous nucleation, which in this case is *lower* by κ from the prediction of classical nucleation theory (CNT) based on the Kelvin curve

$$\kappa = \int_0^{g^*} \ln\left[P_{eq}(g)/P_1(g)\right] dg . \qquad (6.1)$$

In spite of this barrier lowering, g^* and barrier curvature near g^* are the same as in CNT because the location and slope at the crossing point of P_1 with $\ln S_{ext}$ remains the same. Thus the effect of κ is to cause a uniform vertical shift in the barrier relative to CNT, resulting in either a lower (the case depicted here for $\kappa > 0$) or higher ($\kappa < 0$) barrier height: $W^*_{homo} - W^*_{homo}(CNT) = -\kappa kT$. The experimental signature of this effect, in accord with the nucleation theorem, is a vertical shift (also by κ) in curves of $\ln J_{homo}$ versus $\ln S_{ext}$, as is commonly seen in rate measurements [e.g. Strey et al., 1994; Wölk and Strey, 2001]. This effect has been studied using molecular-based theory [McGraw and Laaksonen, 1996] but the present graphical approach makes it more transparent. For the case of *n*-butanol the experimental rate exceeds the CNT prediction by about a factor of 10 [Strey et al. 1994] yielding $\kappa \approx 2-3$. For water the observed shifts (and corresponding values of κ) are smaller and undergo a change in sign at about 240K [Wölk and Strey, 2001].

Substrate-working fluid interactions: Molecular scale interactions between a particle surface and the working fluid can also result in departure from the Kelvin relation. Such interactions are not easily incorporated into macroscopic properties such as the contact angles and line tensions used by CNT. Evidence for strong surface effects that seem to defy a classical description is seen in recent measurements comparing nanometer-sized particles of Ag and NaCl. These substances show very different activation efficiency and, in the case of NaCl, unusual temperature dependence [Schobesberger et al., 2010]. While not complete without a detailed picture of the interactions in question, the graphical method provides a molecular framework for generalization of CNT based on deviations in vapor pressure (positive or negative)

relative to the Kelvin pressure. Figure 8 illustrates the case that departures from classical homogeneous nucleation theory are due to interactions that take place within clusters smaller than the seed, in which case $P_1(g) \approx P_{eq}(g)$ for $g \geq n_{seed}$ and only the interactions between seed and working fluid cause departure from the classical heterogeneous nucleation theory for perfect wetting. The effect on vapor pressure is depicted by the dashed curve $[P = P_2(g)]$ in Fig. 8 for the case of attractive interactions and a vapor pressure lowering near the seed surface. The reduction in h suggested in the figure might possibly be inferred through measurements of the relative sensitivity of heterogeneous nucleation rate to seed size using the nucleation theorem of Eq. 4.14. Note, however, that whenever the vapor pressure at n_{seed} falls below P_{ext}, h becomes negative. Familiar examples occur in Thompson theory, for charged particles, and in Kohler theory for soluble nuclei. In such cases Eq. 4.14 predicts a relative sensitivity of zero as the particle undergoes spontaneous growth until achieving stable equilibrium at P_{ext}. Considering only positive *h*, the integrated effect of vapor-pressure-lowering interactions is to cause a shift in the heterogeneous nucleation barrier height: $W^*_{hetero} - W^*_{hetero}(CNT) = -\delta kT$, where CNT in parenthesis refers not only to classical nucleation theory but also to perfect wetting. δ is the area indicated in Fig. 8:

$$\delta = \int_{g=n_{seed}}^{g^*} \ln[P_1(g)/P_2(g)]dg. \qquad (6.2)$$

The κ- and δ-type molecular interactions (Eqs. 6.1 and 6.2) result in modification of Eq. 5.1:

$$\frac{J_{homo}}{J_{hetero}} \approx \frac{n_v^{eq}}{N} e^{-A_2} e^{(\kappa-\delta)} \leq 1. \qquad (6.3)$$

The methods use to analyze Eq. 5.1 are readily carried over to Eq. 6.3. Positive values of $\delta - \kappa$ allow for detection of smaller particles. Because measurements suggest that κ is typically quite small (i.e., several *kT*), almost any kind of molecular bonding between the substrate and working fluid should allow for the detection of smaller particles than predicted by Eq. 5.1. The opposite tendency, requiring a larger particle sizes for the same detection efficiency, follows for repulsive interactions ($\delta < 0$) - including interactions of the type that manifest macroscopically as cases of imperfect wetting.

The results in this section show both qualitatively and quantitatively how molecular interactions that lower (elevate) vapor pressure cause enhancement (reduction) of nucleation rate. For the ternary organic acid/sulfuric acid/water systems discussed in Sec. 5, recent quantum chemical calculations point to strong organic acid–sulfuric acid hydrogen bonding as responsible for stabilization of the critical complex and enhancement of the nucleation rate seen in laboratory measurements [Zhao et al., 2009].

7. Summary and discussion

In this paper we presented theory and a graphical method for analysis of homogeneous and heterogeneous nucleation barriers. The results reproduce classical nucleation theory for the case that droplet vapor pressure follows the Kelvin relation while allowing interactions at the molecular scale that cause deviations in vapor pressure from the Kelvin result to be formally included. Several nucleation theorems were shown to follow immediately from the graphical method as does the Zeldovich factor, here related to the slope of the Kelvin curve at the critical nucleus size, that appears in expressions for homogeneous and heterogeneous nucleation rate.

Calculations based on mean first passage time kinetics were carried out and used as the benchmark to develop and test a new simplified expression for the MFPT and heterogeneous nucleation rate. Including (or not including in the case of heterogeneous nucleation) Courtney's $1/S$ correction and allowing for particle-vapor association at pre-critical levels of condensate yielded accuracies of a few percent when compared with the MFPT results.

Criteria for guiding the selection of working fluids and operating conditions in order to optimize neutral particle detection were derived from a consideration of detection efficiency and a new metric for assessing heterogeneous nucleation – signal to noise ratio. Corresponding states correlations, previously developed in the context of homogeneous nucleation theory, were show to be applicable to heterogeneous nucleation and used to identify key scaling parameters and obtain results in universal (material independent) form. Detection at minimal seed to molecular volume ratio, $v_{seed}/v_1 = n_{seed}^{min}$ was shown to be favored for larger values of Ω/T, lower vapor concentration, n_v^{eq}, and molecular-level particle-working fluid interactions that lower vapor pressure relative to the Kelvin curve. In the latter case, to the extent these interactions (e.g. hydrogen bonding interactions) are favored and characteristically paired (e.g. antigen-antibody interactions), highly selective methods for nanoparticle detection based on nucleation and growth should result. Future research should include extending the graphical method (or equivalent) to multi-component working fluids, more complete development of molecular-based approaches to nucleation theory using these methods, and theory and experiment aimed at elucidating temperature dependence.

Acknowledgments

This research was supported by the Atmospheric System Research (ASR) Program of the U.S. Department of Energy. We thank Ernie Lewis for valuable discussions.

References

Abraham, F. F. (1974). Homogeneous Nucleation Theory (Academic, New York), Chapt. 5.

Becker C., and Reiss, H. (1978). Estimation of thermophysical properties of a large polar molecule and application to homogeneous nucleation of *l*-menthol, J. Chem. Phys. 68, 3585-3594.

Courtney, W. G. (1961). Remarks on homogeneous nucleation, J. Chem. Phys. **35**, 2249-2250.

Fletcher, N. H. (1958). Size effect in heterogeneous nucleation, J. Chem. Phys. **29**, 572-576.

Gibbs, J. W. (1906). The Scientific Papers of J. Willard Gibbs (Longmans, Green, and Co., London) Vol. 1, pg. 258.

Hale, B. N. (1992). The scaling of nucleation rates, Metallurgical Trans. **23A**, 1863-1868.

Hänggi, P., Talkner, P., Borkovec, M. (1990). Reaction rate theory: fifty years after Kramers, Rev. Mod. Phys. **62**, 251-341.

Iida, K., Stolzenburg, M. R., and McMurry, P. H. (2009). Effect of working fluid on sub-2nm particle detection with a laminar flow ultrafine condensation particle counter, Aerosol Sci. Technol. **43**, 81-96.

Jiang, J., et al. (2010). Electrical mobility spectrometer using a diethylene glycol condensation particle counter for measurement of aerosol size distributions down to 1 nm, Aerosol Sce. Technol., **45**, 510-521.

Kashchiev, D. (1982). On the relation between nucleation work, nucleus size, and nucleation rate, J. Chem. Phys. **78**, 5098-5102.

Katz, J. L., Saltsburg, H., and Reiss, H. (1966). Nucleation in associated vapors, J. Coll. Interface Sci. **21**, 560-568.

Magnusson, L.-E., Koropchak, J. A., Anisimov, M. P., Poznjakovskiy, V. M., and Fernandez de la Mora, J. (2003). Correlations for vapor nucleating critical embryo parameters, J. Phys. Chem. Ref. Data **32**, 1387- 1410.

McGraw, R. (1981). A corresponding states correlation of the homogeneous nucleation thresholds of supercooled vapors, J.. Chem. Phys. **75**, 5514-5521.

McGraw, R. (2001). Dynamics of barrier crossing in classical nucleation theory, J. Phys. Chem. B **105**, 11838-11848.

McGraw, R., and Laaksonen, A. (1996). Scaling properties of the critical nucleus in classical and molecular-based theories of vapor-liquid nucleation, Phys. Rev. Letts. **76**, 2754-2757.

McGraw, R., and Wu, D. T. (2003). Kinetic extensions of the nucleation theorem, J. Chem. Phys. **118**, 9337-9347.

McGraw, R., and Zhang, R. (2008). Multivariate analysis of homogeneous nucleation rate measurements. Nucleation in the p-toluic acid/sulfuric acid/water system, J. Chem. Phys. **128**, 064508, 1- 9.

McGraw, R., and Lewis, E. R. (2009). Deliquescence and efflorescence of small particles, J. Chem. Phys. **131**, 194705, 1-14.

Rasmussen, D. H., and Babu, S. V. (1984). A corresponding states correlation for nucleation from the vapor, Chem. Phys. Letts. **108**, 449-451.

Reiss, H. (1996). Methods of Thermodynamics (Dover, Mineola), pg. 163.

Reiss, H., Marvin, D. C., and Heist, R. H. (1977). The use of nucleation and growth as a tool in chemical physics, J. Coll. Interface Sci. **38**, 125-141.

Rudek, M. M., Fisk, J. A., Chakarov, V. M., and Katz, J. L. (1996). Condensation of a supersaturated vapor. XII. The homogeneous nucleation of the *n*-alkanes, J. Chem. Phys. **105**, 4707-4713.

Schobesberger, S., Winkler, P. M., Pinterich, T., Vrtala, A., Kulmala, M., and Wagner, P. E. (2010). Experiments on the temperature dependence of heterogeneous nucleation on nanometer-sized HaCl and Ag particles, ChemPhysChem **11**, 3874-3882.

Sipilä, M., et al. (2009). Laboratory verification of PH-CPC's ability to monitor atmospheric sub-3 nm clusters, Aerosol Sci. Technol., **43**, 126-135.

Strey, R., Wagner, P. E., and Viisanen, Y. (1994). The problem of measuring homogeneous nucleation rates and the molecular contents of nuclei: Progress in the form of nucleation pulse measurements, J. Chem. Phys. **98**, 7748-7758.

Vanhanen, J., et. al., (2010). Particle size magnifier for nano-CN detection, Aerosol Sci. Technol., **45**, 533-542.

Vehkamäki, H., Määttänen, A., Lauri, A., Napari, I., and Kulmala, M. (2007). Technical Note: The heterogeneous Zeldovich factor, Atmos. Chem. Phys. **7**, 309-313.

Wedekind, J., Strey, R., and Reguera, D. (2007). New method to analyze simulations of activated processes, J. Chem. Phys. **126**, 134103, 1-12.

Winkler, P. M., Steiner, G., Vrtala, A., Vehkamäki, H., Noppel, M., Lehtinen, K. E. J., Reischl, G. P., Wagner, P. E., and Kulmala, M. (2008). Heterogeneous nucleation experiments bridging the scale from molecular ion clusters to nanoparticles, Science **319**, 1374-1377.

Wölk, J., and Strey, R. (2001). Homogeneous nucleation of H_2O and D_2O in comparison: The isotope effect, J. Phys. Chem. B **105**, 11683-11701.

Zhang, R., Suh, I., Zhao, J., Zhang, D., Fortner, E. C., Tie, X., Molina, L. T., and Molina, M. J. (2004), Atmospheric new particle formation enhanced by organic acids, Science **304**, 1487-1490.

Zhang, R., Wang, L., Khalizov, A. F., Zhao, J., Zheng, J., McGraw, R., and Molina, L. T. (2009), Formation of nanoparticles of blue haze enhanced by anthropogenic pollution, Proc. Natl. Acad. Sci. **106**, 17650-17654.

Zhao, J., Khalizov, A., Zhang, R., and McGraw, R. (2009), Hydrogen-boding interaction in molecular complexes and clusters of aerosol nucleation precursors, J. Phys. Chem. A **113**, 680-689.

Property	*l*-menthol	*n*-nonane	*n*-butanol	water
S_{cr}	111.5	7.41	3.11	3.20
$T(K)$	323.15	300	300	298.15
Ω / T	4.19	2.40	1.64	1.69
g^*	23.6	57.8	101.6	102.2
W^*_{homo} / kT	55.5	57.9	57.7	59.5
$n_v^{eq}(cm^{-3})$	1.19×10^{16}	1.57×10^{17}	2.58×10^{17}	7.69×10^{17}
$f^{miin}(N=1)$	0.230	0.244	0.254	0.251
$h(f^{min})$	2.98	1.20	0.66	0.68
n^{min}_{seed}	5.4	14.1	25.8	25.7
$v_1(cm^3)$	2.38×10^{-22}	2.99×10^{-22}	1.53×10^{-22}	3.00×10^{-23}
$d^{min}_{seed}(nm)$	1.35	2.00	1.96	1.14

Table 1. Parameters and scaling properties for the four working fluids included in Fig. 7 and the theoretical minimum particle size (d^{min}_{seed}) that can be detected by each for $N = 1cm^{-3}$. Data sources: *l*-menthol, Becker and Reiss (1978); *n*-nonane, Rudek et al. (1996); *n*-butanol, Magnusson et al. (2003); water: Wölk and Strey (2001).

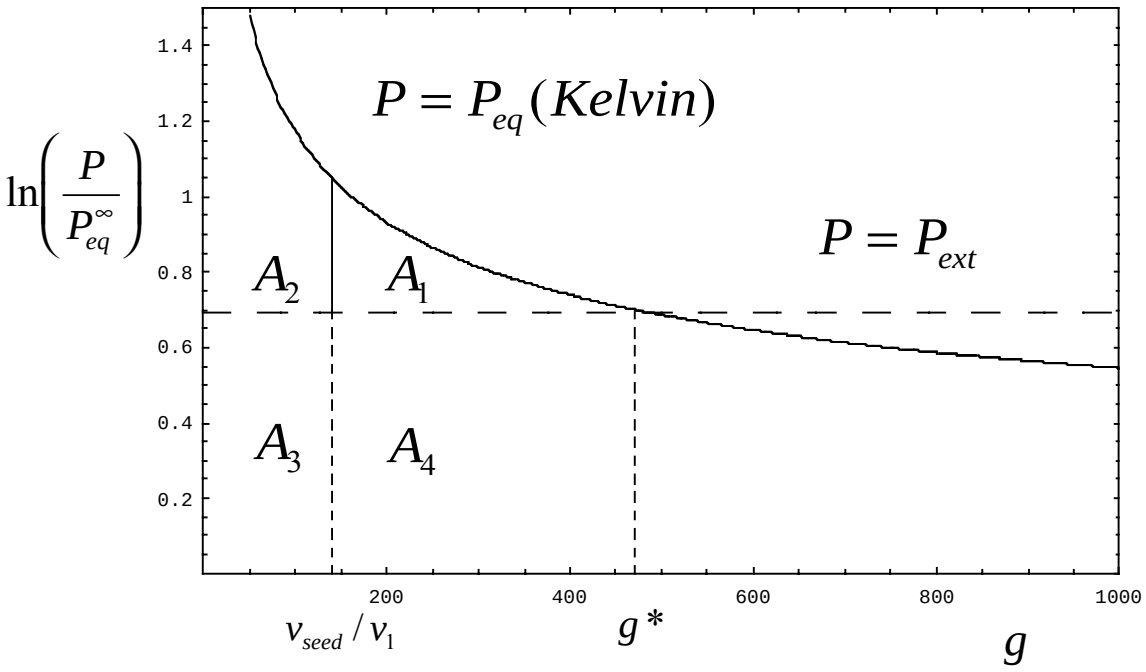

Figure 1. Area constructions derived from the Kelvin curve. Solid curve is the Kelvin curve for water from Eq. 2.1. Horizontal dashed line is for a water vapor saturation ratio of 2 (relative humidity = 200%). The point of intersection marks the critical drop size, $g*$ consisting of the seed particle plus $n* = g* - v_{seed} / v_1$ molecules of condensed water. See text for interpretation of labeled areas $A_1 - A_4$.

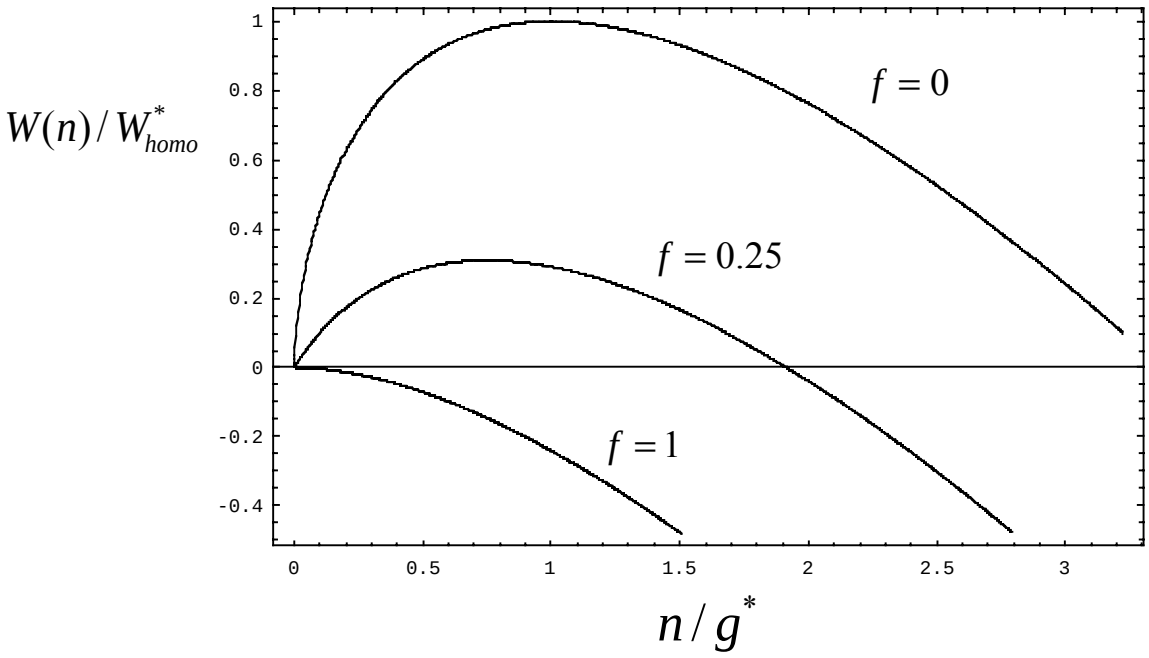

Figure 2. Scaled nucleation barrier profiles from Eq. 2.7 for several seed volume fractions ($f = n_{seed}/g^*$). Curves top to bottom: homogeneous nucleation case ($f = 0$), an intermediate heterogeneous nucleation case ($f = 0.25$), and the Kelvin limit ($f = 1$).

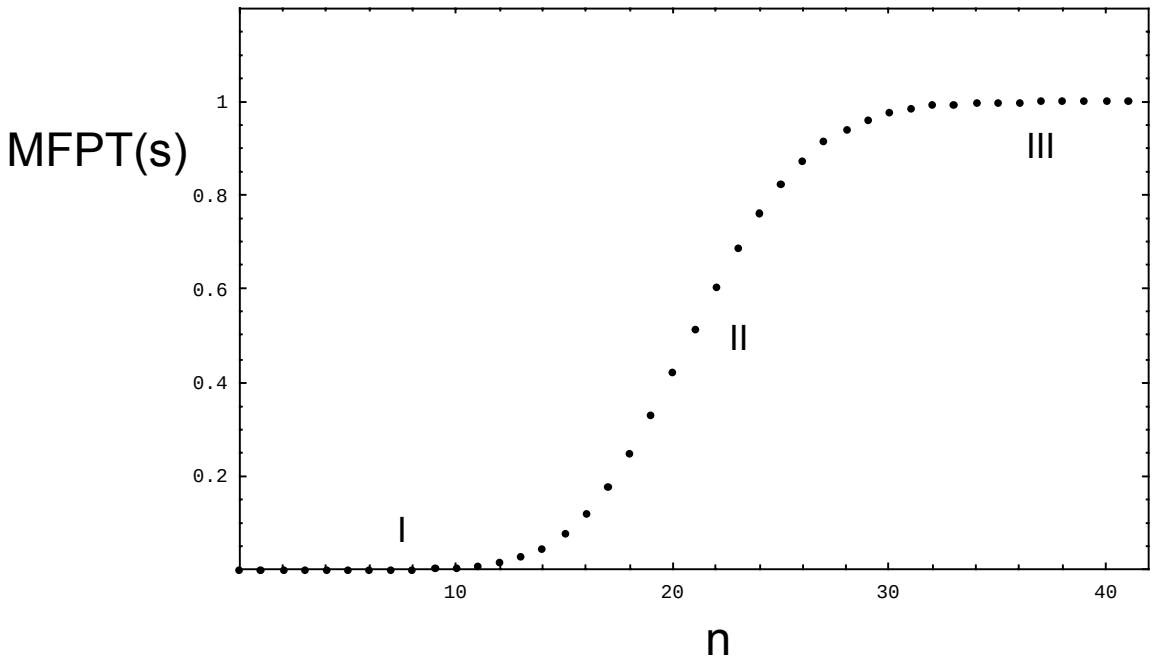

Figure 3. Typical behavior of the mean first passage time (MFPT) to reach a given cluster size as a function of that size. n is the number of molecules condensed onto the seed. Region I, quasi-equilibrium between clusters of pre-critical size. Region II, inflection point at the critical size. Region III, rapid growth regime. Calculations are for heterogeneous nucleation of *l*-menthol on a 1.5nm diameter seed. $S_{ext} = 86.0$, $W^* / kT = 18.1,\ J_1 = 1.$

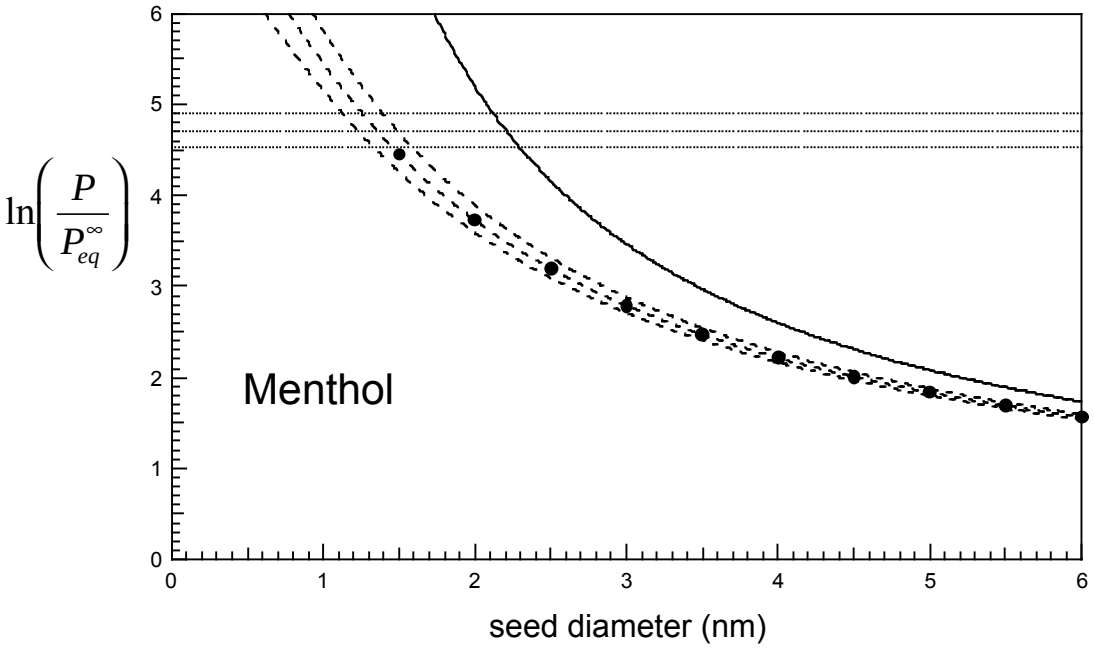

Figure 4. Nucleation rates for menthol. Solid curve is the Kelvin limit. Dashed lines and curves are contours of constant nucleation rate. Horizontal lines: contours of constant homogeneous nucleation rate for, top to bottom, $J_{homo} =$ 100, 1, and 0.01 $cm^{-3}s^{-1}$. Dashed curves give similar contours for the heterogeneous nucleation rate from the new approximate prefactor-exponent form: top to bottom, $J_{homo} =$ 100, 1, and 0.01 cm $^{-3}$s^{-1}. Markers: results from the double summation calculation for mean first passage time and $J_1 = 1\, cm^{-3}s^{-1}$. These show excellent agreement with the approximate result (middle curve).

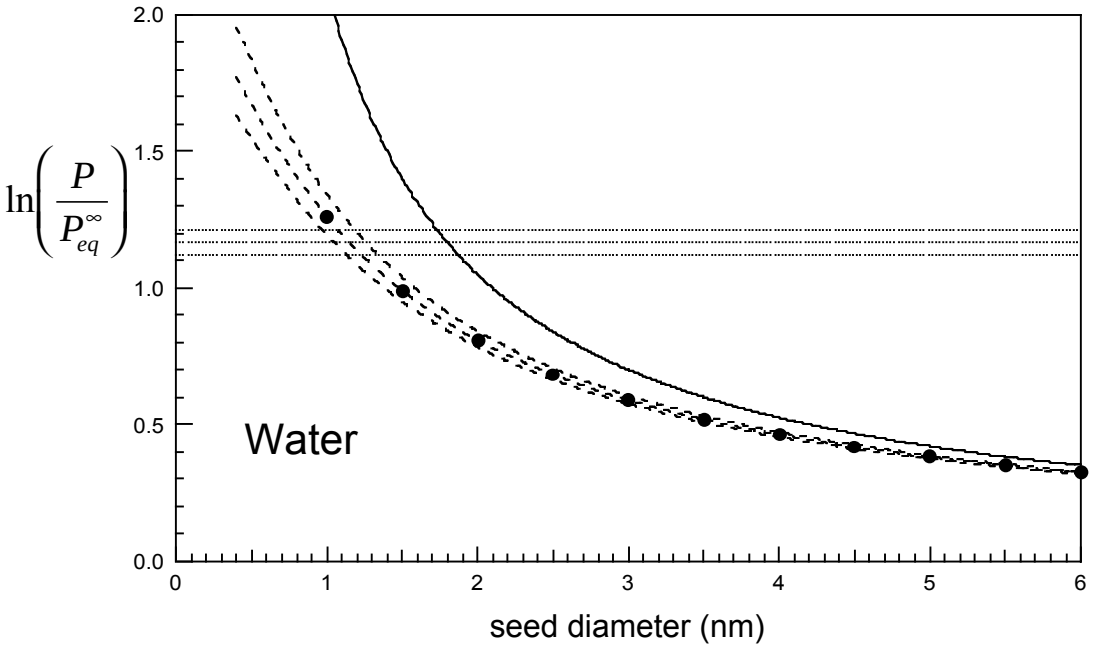

Figure 5. Nucleation rates for water. Solid curve is the Kelvin limit. Dashed lines and curves are contours of constant nucleation rate. Horizontal lines: contours of constant homogeneous nucleation rate for, top to bottom, $J_{homo} = 100$, 1, and 0.01 $cm^{-3}s^{-1}$. Dashed curves give similar contours for the heterogeneous nucleation rate from the new approximate prefactor-exponent form: top to bottom, $J_1 =$ 100, 1, and 0.01 $cm^{-3}s^{-1}$. Markers: results from the double summation calculation for mean first passage time and $J_1 = 1\, cm^{-3}s^{-1}$. These show excellent agreement with the approximate result (middle curve).

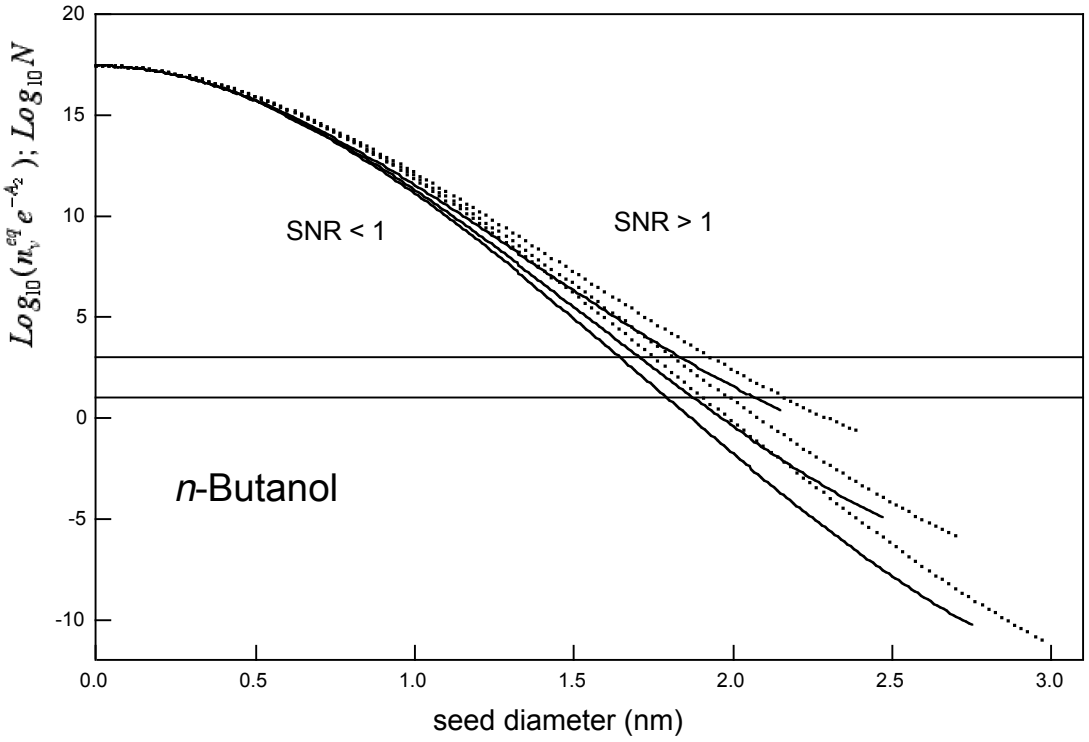

Figure 6. Curves of equal heterogeneous and homogeneous nucleation rates $(SNR = 1)$ for *n*-butanol. Logarithm of $n_v^{eq} e^{-A_2}$ or N (these are equal along these curves) versus seed diameter (nm). Solid curves: $T = 300K$; top to bottom $J = 10^6$ $(S_{ext} = 3.67)$, 1 $(S_{ext} = 3.11)$, 10^{-6} $(S_{ext} = 2.78)$. Dashed curves: $T = 320K$, top to bottom $J = 10^6$ $(S_{ext} = 2.87)$, 1 $(S_{ext} = 2.56)$, 10^{-6} $(S_{ext} = 2.31)$. Results are shown for $d_{seed} / d_{Kelvin} < 0.8$ beyond which the barrier height is lower than $5kT$. Signal-to-noise ratios for a given set of conditions exceed (are less than) unity to the right and above (left and below) the corresponding curve. Horizontal lines: typical range for N $(= 10^1 - 10^3 cm^{-3})$ in CPC measurements.

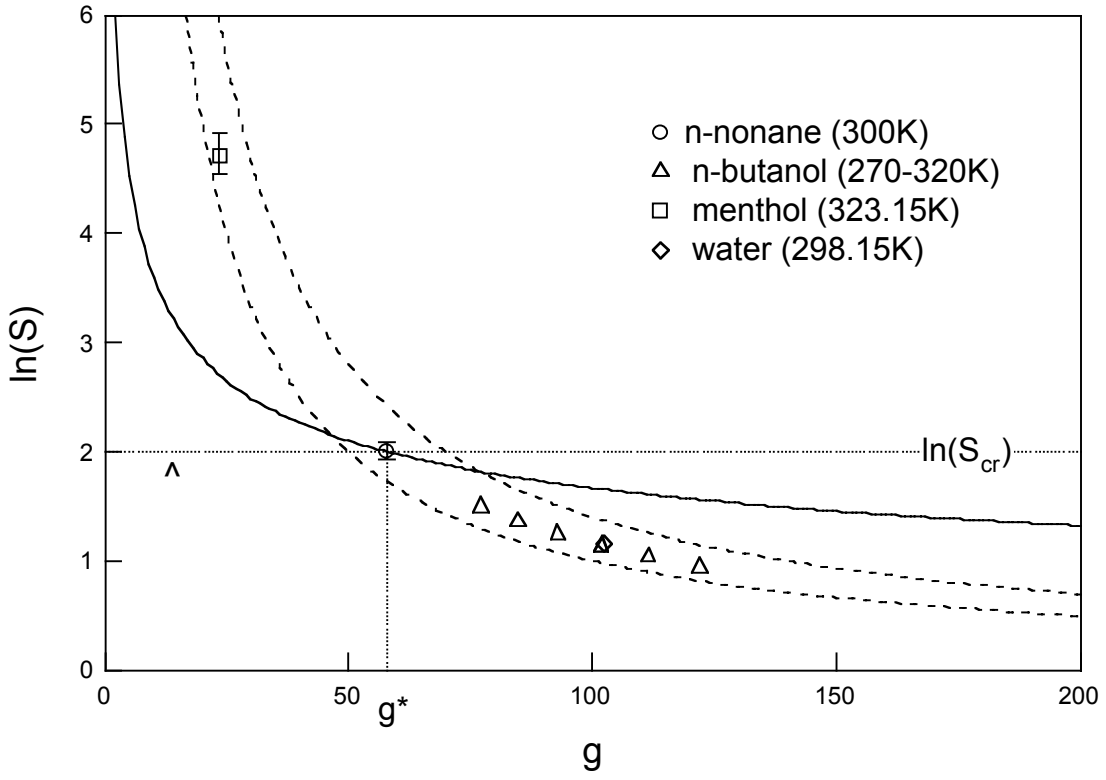

Figure 7. Scaled nucleation rate. Dashed hyperbolic curves: contours of constant homogeneous nucleation barrier height, 50 kT (lower curve) and 70 kT (upper curve). The region between these curves provides a good indication of homogeneous nucleation threshold range for most substances. Markers show four candidate working fluids and are centered on critical cluster size and the critical saturation ratio, which for each fluid gives $J_{homo} = 1$. Error bars show a four order of magnitude range in nucleation rate from $J_{homo} = 0.01$ to 100. No error bar means that the height of the symbol itself exceeds this range. The solid curve is the Kelvin curve for nonane ($\Omega / T = 2.40$ at $T = 300K$). The horizontal and vertical dotted lines for nonane mark the logarithm of its critical saturation ratio $\ln(S_{cr})$ and g^*, respectively. The area of the rectangle bounded by these lines and the axes is twice the reduced barrier height, W^*_{homo} / kT. The caret marks the $N = 1$ detection limit for nonane.

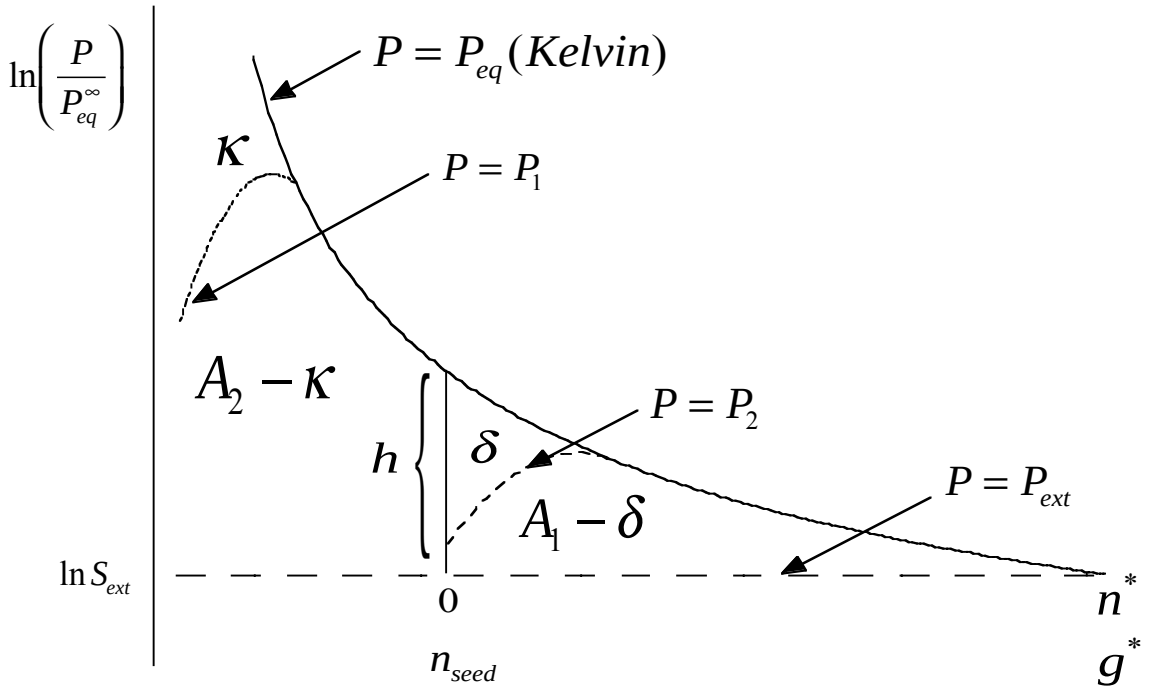

Figure 8. Area construction similar to Fig. 1 but illustrating the effect of interactions that lower the equilibrium vapor pressure relative to the Kelvin curve (solid curve). The dotted curve, which only departs from Kelvin at the smallest cluster sizes, results in a lowering of the barrier height for homogeneous nucleation to $A_1 + A_2 - \kappa$. The dashed curve shows lowering of the heterogeneous barrier from A_1 to $A_1 - \delta$. h is the length of the vertical line segment given by Eq. 4.5. Note that the abscissa (upper scale) has been shifted in the heterogeneous case to tally only the number of molecules of condensed working fluid. The lower scale, which runs out to g^* applies to the homogeneous case.

.